Demonstration of a light-driven SO_4^{2-} transporter and its spectroscopic characteristics

Akiko Niho[1, +], Susumu Yoshizawa[2, +], Takashi Tsukamoto[1,3, +], Marie Kurihara[3], Shinya Tahara[4], Yu Nakajima[2], Misao Mizuno[5], Hikaru Kuramochi[4,6], Tahei Tahara[4,6], Yasuhisa Mizutani[5] & Yuki Sudo[1,3, *]

[1]Division of Pharmaceutical Sciences, Okayama University, Okayama 700-8530, Japan.
[2]Atmosphere and Ocean Research Institute, University of Tokyo, Chiba 277-8564, Japan.
[3]Graduate School of Medicine, Dentistry and Pharmaceutical Sciences, Okayama University, Okayama 700-8530, Japan.
[4]Molecular Spectroscopy Laboratory, RIKEN, 2-1 Hirosawa, Wako 351-0198, Japan.
[5]Department of Chemistry, Graduate School of Science, Osaka University, 1-1 Machikaneyama, Toyonaka, Osaka 560-0043, Japan
[6]Ultrafast Spectroscopy Research Team, RIKEN Center for Advanced Photonics (RAP), 2-1 Hirosawa, Wako 351-0198, Japan

[+]These authors contributed equally to this work.

[*]To whom correspondence should be addressed. Yuki Sudo; Email: sudo@okayama-u.ac.jp

KEYWORDS: membrane protein; ion transport; divalent anion; isomerization

ABSTRACT

In organisms, ion transporters play essential roles in the generation and dissipation of ion gradients across cell membranes. Microbial rhodopsins selectively transport cognate ions using solar energy, in which the substrate ions identified to date have been confined to monovalent ions such as H^+, Na^+ and Cl^-. Here we report a novel rhodopsin from the cyanobacterium *Synechocystis* sp. PCC 7509, which inwardly transports a polyatomic divalent sulfate ion, SO_4^{2-}, with changes of its spectroscopic properties both in unphotolyzed and photolyzed states. Upon illumination, cells expressing the novel rhodopsin, named *Synechocystis* halorhodopsin (SyHR), showed alkalization of the medium only in the presence of Cl^- or SO_4^{2-}, That alkalization signal was enhanced by addition of a protonophore, indicating an inward transport of Cl^- and SO_4^{2-} with a subsequent secondary inward H^+ movement across the membrane. The anion binding to SyHR was suggested by absorption spectral shifts from 542 nm to 536 nm for Cl^- and from 542 nm to 556 nm for SO_4^{2-}, and the affinities of Cl^- and SO_4^{2-} were estimated as 0.112 mM and 5.81 mM, respectively. We then performed time-resolved spectroscopic measurements ranging from femtosecond to millisecond time domains to elucidate the structure and structural changes of SyHR during the photoreaction. Based on the results, we propose a photocycle model for SyHR in the absence or presence of substrate ions with the timing of their uptake and release. Thus we demonstrate SyHR as the first light-driven polyatomic divalent anion (SO_4^{2-}) transporter and report its spectroscopic characteristics.

INTRODUCTION

Organisms utilize light not only as signals, but also as an energy source. Such biological activities are established by the functions of various photoactive proteins. Seven-transmembrane α-helical proteins, called "rhodopsins or retinal proteins", have a vitamin-A aldehyde retinal as a chromophore via a protonated Schiff base linkage with a conserved specific Lys residue in the 7^{th} (G-) helix.[1] Since 2000, metagenomic studies have revealed that rhodopsins are widely distributed in the microbial world.[2] Light absorption by microbial rhodopsins commonly triggers a *trans-cis* isomerization of the retinal chromophore and the stored energy of the excited retinal chromophore induces sequential conformational changes of the protein moiety.[1] Among microbial rhodopsins, light-driven ion pumps form huge phylogenetic clusters not only in archaea and eubacteria but also in eukaryotes (Figure 1A).[3,4] For ion pumps, during a sequential photoreaction cycle called the photocycle, ions are transported across the membrane from/to the extracellular (EC) side or the cytoplasmic (CP) side.

In 1971, Oesterhelt and Stoeckenius identified a light-driven proton (H^+) pumping rhodopsin from the archaeon *Halobacterium salinarum* (formerly *halobium*).[5] They named that protein *H. salinarum* bacteriorhodopsin (HsBR) (Figure 1A), and the direction of the H^+ translocation has been determined to be from the CP to the EC side.[1] In 1980, a light-driven inward chloride ion (Cl^-) pump was discovered in the archaeon *H. salinarum*.[6] Functionally, that protein, named *H. salinarum* halorhodopsin (HsHR), is the mirror image of HsBR: an anion rather than a cation is transported, and the translocation is from the EC to the CP direction.[1] Another HR from a highly haloalkaliphilic archaeon *Natronomonas* (formerly *Natronobacterium*) *pharaonis* (NpHR) was discovered in 1986 (Figure 1A).[7] The photoexcitation of HRs results in the sequential appearance of various photointermediates (K, L, N and O), followed by a return to the unphotolyzed form, as occurs in HsBR, except for the lack of the M-like blue-shifted intermediate.[8] Of note, for the H^+ pumps, the H^+ can be transferred through several functional groups by the Grotthuss mechanism, but direct ion translocation is required for the Cl^-. It is known that the retinal Schiff base of HRs is protonated, as in HsBR, but the counterion Asp85 in HsBR, which is essential for the H^+ pump function, is replaced by a neutral Thr residue in HRs (Figure 1B). For HsBR, the H^+ of the protonated Schiff base is transferred to the nearby deprotonated counterion Asp85 upon formation of the M intermediate, and therefore the photocycle of HR lacks the M intermediate.[1] The high-resolution crystal structures of HsHR and NpHR were reported in 2000 and 2010, [9,10] respectively. Those structures both showed that the Schiff base region contains a quadrupole with positive charges, and counterbalancing negative charges located at the Cl^- and an Asp residue. From the spectral shift in the visible region upon Cl^- binding, the affinity of the Cl^- is estimated to be about 10 mM and 2.5 mM for HsHR and NpHR, respectively.[11,12] Upon formation of the K intermediate,

the Cl^- follows the flipped dipole of the N–H Schiff base bond, and forms a strong hydrogen bond with the protonated Schiff base. The opening of an EC pathway from the CP release site towards the protein surface was attributed either to a spectroscopically silent transition between two L-like intermediates or an L-O transition.[13-15] According to stopped-flow studies of NpHR, Cl^- uptake itself is mostly regulated by passive diffusion through an EC pathway during later stages of the photocycle.[16]

Thus, for the ion transporters, the substrate ions identified to date have been confined to monovalent ions such as H^+ and Cl^-.[1] In other words, no divalent ion transporting rhodopsin has been discovered so far. In this study, to identify a rhodopsin-based divalent ion transporter, we focused on a putative rhodopsin molecule (Protein accession no. WP_009632765) from the cyanobacterium *Synechocystis* sp. PCC 7509 (Genome accession no. ALVU00000000). That cyanobacterium was isolated from rock scrapings containing sulfate rich minerals at Schöllenene Gorge in Switzerland.[17,18] That rhodopsin, named *Synechocystis* halorhodopsin (SyHR), is phylogenetically distinct from H^+ pumps, such as HsBR, proteorhodopsin (PR) and thermophilic rhodopsin (TR), and from Cl^- pumps, such as *Nonlabens marinus* rhodopsin 3 (NM-R3) and *Fluvimarina pelagi* rhodopsin (FR) (Figure 1A). SyHR was categorized as a cyanobacterial Cl^- pump, as is HR from *Mastigocladopsis repens* PCC 10914 (MrHR; Protein accession no. WP_017314391).[19] Comparison of their amino acid sequences revealed that SyHR and MrHR share a characteristic T (Thr) – S (Ser) – D (Asp) motif on the 3rd (C-) helix, where T, S and D correspond to Asp85, Thr89 and Asp96 in HsBR, respectively (Figure 1B). Among them, two aspartates in HsBR, Asp85 and Asp96, play important roles in stabilizing the protonated Schiff base in the dark as a counterion and in proton donation of the deprotonated Schiff base during the photocycle, respectively,[20] while Thr89 stabilizes deprotonated Asp85 through the hydrogen bonding network.[21] Of note, light-induced pH change experiments revealed that MrHR transports monovalent ions including Cl^- and Br^- but not SO_4^{2-} upon illumination.[19] The putative secondary structural analysis of SyHR shows seven (A, B, C, D, E, F and G) transmembrane α-helices with short β-sheets between the B and C helices as occurs in HsHR and NpHR (Figure 1C). On the basis of that background, here we report the newly discovered rhodopsin SyHR that transports a polyatomic divalent anion SO_4^{2-}. In short, we succeeded in expressing SyHR in *Escherichia coli* (*E. coli*) as a recombinant protein and then characterized the photobiological and photochemical properties of SyHR and compared them with the other microbial anion pumping rhodopsins, MrHR, HsHR and NpHR.

MATERIALS AND METHODS

The codon-optimized SyHR was chemically synthesized by Eurofins Genomics (Tokyo, Japan) and was inserted into the pET21a plasmid vector (Novagen, Madison, WI, USA) to express the

protein in *Escherichia coli* BL21(DE3). The procedure and apparatus for light-induced pH change measurements were essentially the same as reported previously.[22] For protein purification, the SyHR-expressing cells were solubilized with 1.5% (w/v) n-dodecyl-β-D-maltoside (DDM, Dojindo Lab., Kumamoto, Japan) and the solubilized SyHR was purified by a HisTrap FF Ni^{2+}-NTA affinity chromatography column (GE Healthcare, Amersham Place, England). The sample medium was replaced with the appropriate buffer solution by passage over a PD-10 size-exclusion column (GE Healthcare). The retinal isomer compositions were analyzed by normal phase HPLC using an LC-20AT chromatography system equipped with a SPD-20A photodetector (Shimadzu, Kyoto, Japan) and a YMC-Pack SIL 6.0 × 150 mm chromatography column (YMC, Kyoto, Japan) as described previously.[23]

UV-visible absorption spectra were recorded at room temperature using a UV-1800 spectrophotometer (Shimadzu). The affinity constant of each anionic substrate was estimated by fitting the data to the Hill equation. For the pH titration experiments, the sample was initially suspended in water containing 6 reagents (0.89 mM citrate, 0.89 mM MES, 1.1 mM TES, 0.78 mM TAPS, 1.1 mM CHES and 0.33 mM CAPS) [24] and 0.05% DDM with 1 M NaCl or 333 mM Na_2SO_4. The acid dissociation constant (pK_a) was estimated by fitting the data to the Henderson-Hasselbalch equation. Apparatus and procedures of the resonance Raman (RR) spectroscopy and time-resolved absorption spectroscopy are provided in Supporting Information with details of experimental materials and methods.

RESULTS

Anion transport activity of SyHR

From its position on the phylogenetic tree of rhodopsins (Figure 1A) and the amino acid sequence alignment (Figure 1B), it was assumed that SyHR works as a light-driven inward anion transporter. In fact, SyHR shares a high sequence similarity with MrHR (68% identity, 91% similarity), which was recently reported as a light-driven inward anion pump.[19] We measured the light-induced pH changes of suspensions of *E. coli* cells expressing SyHR to identify its ion transport activity (Figure 2). The expression of SyHR was successfully confirmed by the pink color of the *E. coli* cells. For all cells expressing proton pumping rhodopsins such as TR, light-induced decreases in pH have been observed, and the presence of the protonophore CCCP strongly impaired those pH changes.[22] However, a light-induced increase in pH was observed for SyHR in a solution containing 100 mM NaCl (grey dotted line) and that signal was enhanced by the addition of 10 μM CCCP (black solid line) (Figure 2A). The altered pH recovered to the original pH within a few minutes after turning off the light. Because CCCP is a proton-selective ionophore, the pH gradient between the inside and the outside of the cell membrane disappeared before the illumination. Therefore, we assumed that

the signal corresponds to the transportation of some anions or cations with a subsequent secondary inward H^+ movement across the membrane. Thus, SyHR is considered to be a light-dependent outward Na^+ or inward Cl^- transporter. Next, to identify the substrate ion(s) of SyHR, we performed similar experiments in solutions containing different monovalent salts, NaBr, NaI, KCl or $NaNO_3$. The signal almost disappeared in solutions containing NaI or $NaNO_3$, suggesting that Na^+ is not a substrate ion, while strong signals were observed in solutions containing NaBr or KCl, suggesting that Br^- can be a substrate ion as well as Cl^- (Figures 2A and 2B). Thus, these data indicate that SyHR is a light-driven anion transporter. It is noteworthy that a light-induced increase in pH and its enhancement by the addition of CCCP were also observed for SyHR in a solution containing 100 mM Na_2SO_4 (Figure 2B). For anion transporters, Na_2SO_4 is widely used as a standard non-substrate salt because of its characteristic that SO_4^{2-} is a large polyatomic divalent ion. In fact, no light-induced pH change has been observed for SO_4^{2-} in the other anion transporting rhodopsins including MrHR.[19] It should be noted that, in our experimental conditions (pH 5 - 7), sulfate ions exist as a divalent form (SO_4^{2-}) but not as a monovalent form (HSO_4^-) judged by its pKa value (ca. 1.9) (Figure 2C).[25] These results strongly suggest that SyHR characteristically transports not only monovalent anions (Cl^- and Br^-) but also a divalent SO_4^{2-} anion. Incidentally, the enhanced signals in the presence of CCCP completely disappeared following the addition of tetraphenylphosphonium ion (TPP^+), which is a hydrophobic cationic reagent that disrupts the membrane potential (Figure 2B).[26]

Anion binding to SyHR

To investigate the effects of the substrate ions (Cl^- and SO_4^{2-}) on the spectroscopic properties of SyHR, we measured UV-visible absorption spectra of purified SyHR in the presence or absence of 1 M NaCl or 1 M Na_2SO_4. Here we employed the MOPS buffer for which the pH was adjusted by the addition of NaOH. Because Cl^- and SO_4^{2-} are the substrates for SyHR, buffers for which the pH is adjusted from basic to neutral by addition of HCl or H_2SO_4 are not suitable in this study. In addition, at neutral pH around 7, a partial deprotonation of the retinal Schiff base was observed especially for SyHR in the presence of SO_4^{2-} (ca. 5%) due to its smaller pK_a value (see following section and Figure 5G). To maintain the retinal Schiff base completely protonated, the pH was adjusted to ca. 5. The λ_{max} of SyHR was clearly shifted from 542 nm to 536 nm or to 556 nm by the addition of NaCl or Na_2SO_4 to the desalted buffer solution, respectively (Figure 3A). It should be noted that such a SO_4^2-induced spectral shift was not observed in any other microbial rhodopsins,[12,19,27] indicating that it is characteristic for SyHR (Table 1). To confirm whether the spectral change was caused by a difference in the retinal configuration, we performed HPLC analysis, since it is well known that an increase in the 13-*cis* retinal oxime isomer causes a spectral blue shift in microbial rhodopsins.[28,29] As shown in

Figure 3B, SyHR predominantly contained an all-*trans* retinal as its chromophore both in the presence or absence of salts (w/o salt: 94.1%, 1 M NaCl: 97.5%, 1 M Na_2SO_4: 96.1%), indicating that the spectral shift of SyHR is not caused by a change in the retinal configuration. Thus the anion-induced spectral shifts likely represent an environmental change around the chromophore, leading to an increase or a decrease in the energy gap between the electronic ground and excited states for the blue and the red shifts, respectively. These spectral shifts without a change of the retinal composition allowed us to perform anion titration experiments. Figures 3C and E show the spectral changes over a wide salt concentration range from 0 to 1 M. As shown in Figures 3D and F, the difference spectra show isosbestic points at around 550 nm both for NaCl and for Na_2SO_4, indicating there is an equilibrium between the anion-bound and anion-unbound forms in SyHR. The absorbance changes at 592 nm were plotted against the salt concentrations (Figure 3G), and the affinity constants (K_d) were estimated using the Hill equation as 0.112 ± 0.0166 mM for Cl^- (blue circles) and 5.81 ± 1.40 mM for SO_4^{2-} (red circles). These values are comparable to those of other anion pumps such as MrHR (1.99 mM for Cl^-), HsHR (10 mM for Cl^-) and NpHR (2 mM for Cl^-) (Table 1).[11,12,19]

To analyze the possibility of whether the SO_4^{2-} binding site is shared with the Cl^- one, we performed competition experiments. Figure 4 shows the spectral changes of SyHR elicited by the addition of Cl^- or SO_4^{2-} in the presence of 1 M Na_2SO_4 or 1 M NaCl, respectively. The absorption spectrum of SyHR in a solution containing 1 M Na_2SO_4 was clearly shifted to the shorter wavelength in a Cl^--dependent manner (Figure 4A). Both the presence of an isosbestic point at approximately 550 nm in the difference spectra and the high affinity of Cl^- compared to SO_4^{2-} (ca. 40-fold) indicate the transition of SyHR from the SO_4^{2-}-bound form to the Cl^--bound form (Figure 4B). This is supported by the result that the absorption maximum of SyHR in a solution containing 1 M NaCl or 1 M Na_2SO_4 (solid line in Figure 4A) is identical to that with Cl^- alone (i.e., 536 nm, see Figure 3A). On the other hand, the absorption spectrum of SyHR in a solution containing 1 M NaCl is not altered by the addition of SO_4^{2-} (Figures 4C and 4D). This is interpreted in terms of the lower binding affinity of SO_4^{2-} to SyHR than Cl^-. The apparent K_d value for Cl^- in the background of SO_4^{2-} is estimated as 0.0795 mM by the Hill equation (Figure 4E), which is comparable to the K_d value for Cl^- (0.112 mM, Figure 3G). Thus, from these results, we assume that the SO_4^{2-} binding site is shared with the Cl^- binding site.

Estimation of pK_a of the charged group(s) in SyHR

Then we performed a spectroscopic pH titration to estimate the pK_a of the charged residues in SyHR. Under alkaline conditions, large spectral blue-shifts were observed both in the presence and in the absence of salts (Figures 5A, C and E). The difference absorption spectra (Figures 5B, D and F) showed increases in absorbance at about 400 nm with isosbestic points at 460 nm,

indicating the presence of an equilibrium between the protonated and deprotonated forms. It is known that deprotonation of the Schiff base (Lys205) causes a large spectral blue-shift to about 400 nm. Thus, the spectral shift can be assigned to the deprotonation of Lys205 in SyHR upon alkalization. To analyze the transition quantitatively, the absorption changes at 409 nm for no salt or Na_2SO_4 and 397 nm for NaCl were again plotted against the environmental pH and the titration curves were analyzed using the Henderson-Hasselbalch equation with a single pK_a value. From these data, the pK_a values were estimated as 9.48 ± 0.1 for SyHR without salt, 10.6 ± 0.05 for SyHR with Cl^- and 8.82 ± 0.03 for SyHR with SO_4^{2-} (Figure 5G). These values are similar to those of NpHR (Table 1) and are a few units less than those of other microbial rhodopsins,[12,22,30,31] suggesting that there is a hydrophobic environment around the Schiff base in anion transporters including NpHR and SyHR. It should be noted that such a SO_4^{2-}-induced change of the pK_a of the Schiff base has not been reported in any other microbial rhodopsins so far, indicating that it is characteristic for SyHR. Similar experiments were performed under acidic conditions. As a result, a spectral shift was not observed from pH 4 to 7 with or without salts (Figure 5G). This result was interpreted in terms of the lack of the counterion in SyHR (Asp85 in HsBR). In general, the protonated Schiff base of the retinal chromophore in microbial rhodopsins is stabilized by a carboxylate (Asp or Glu) as a counterion,[1,17] however that residue is replaced by a neutral residue such as Thr or Ser in anion transporting microbial rhodopsins including SyHR (Figure 1B), in which the bound anion acts as a counterion.

Resonance Raman spectroscopic analysis of SyHR

To investigate the structure of the retinal chromophore embedded in proteins and its effects on anion binding, we measured resonance Raman (RR) spectra using laser pulses at 532 nm. Figure 6A shows the RR spectra of SyHR without salts (no salt) and with 1 M NaCl (Cl^-) or 333 mM Na_2SO_4 (SO_4^{2-}). The concentrations of anions were judged to be sufficient for the binding to SyHR from the anion titration experiments as demonstrated above (Figure 3G). The red and blue traces represent RR spectra measured in H_2O buffer and in D_2O buffer, respectively. As seen, almost no significant anion dependency was observed for the RR spectra of SyHR, indicating that the structure of the retinal chromophore in SyHR is not altered upon anion binding. Hereafter, all Raman bands for SyHR were interpreted in terms of the assignments for HsBR because the overall spectral features of the observed RR spectra of SyHR were very similar to those of HsBR, whose normal mode analysis has already been carried out in detail.[32]

For the low-frequency region (800-1100 cm^{-1}), the symmetric rocking mode of methyl groups connected to the C9 and C13 atoms of the retinal[33] was observed at 1008 cm^{-1} (Figure 6A). In addition, some weak bands assignable to hydrogen-out-of-plane (HOOP) wagging modes were observed at 824, 840, 880, 898 and 958 cm^{-1}.[34] Curry et al. formulated general rules

for HOOP frequencies in trans-substituted polyenes.[35] Hydrogens trans to a double bond (H-C_7=C_8-H and H-C_{11}=C_{12}-H) couple strongly forming A_u HOOP mode from 950 to 970 cm^{-1} range and B_g HOOP mode from 750 to 850 cm^{-1}. A HOOP mode due to a hydrogen trans to a methyl group across a double bond (C_{10}-H and C_{14}-H) appears between 850 and 900 cm^{-1}. Therefore, the 958-cm^{-1} band is assigned to A_u HOOP mode. It is well-known that the intensity of the HOOP band in rhodopsins is strongly enhanced when the polyene chain of the retinal is distorted.[36] Because A_u HOOP is a symmetric combination of two C-H wagging modes, a Raman band of A_u HOOP mode is particularly enhanced by the distortion. The weak A_u HOOP intensity at 958 cm^{-1} indicates that the polyene chain of the chromophore in SyHR is little distorted. The skeletal C–C stretch bands appearing in a "fingerprint" region (1100-1250 cm^{-1}) are structural markers to determine the geometry of the retinal chromophore.[34] For SyHR, we observed C–C stretch bands at 1167, 1173, 1185, 1202 and 1211 cm^{-1}. These frequencies and spectral shapes were quite similar to those of microbial rhodopsins having the all-*trans* form of the retinal chromophore. Thus we concluded that, in the unphotolyzed state, SyHR has an all-*trans* retinal chromophore either in the presence or the absence of substrate anions, which is consistent with the results of the HPLC measurements shown in Figure 3B.

The frequencies of the strongest C=C stretch bands were similar between the spectra of SyHR with or without Cl^- and SO_4^{2-}. For retinal proteins and model compounds of the retinal chromophore, it is well-known that there is an inverse linear correlation between the C=C stretching frequency and the absorption maximum of the retinal chromophore.[37] Figure 6B depicts a plot of the C=C stretching frequency against the absorption maximum wavelength for 14 retinal proteins.[38-50] The black line represents the best-fit with a linear function for the previous observations.

Raman bands due to the Schiff base were observed at 1639 and 1353 cm^{-1} for SyHR without salt, which are assigned to the C=N stretch and the N-H rocking vibration, respectively (Figure 6A). In D_2O, the C=N stretch band downshifted to 1623 cm^{-1}, while the band at 977 cm^{-1} newly appeared as the N-D rock band with the disappearance of the band at 1353 cm^{-1}. In the protonated Schiff base of the retinal chromophore, the C=N stretching vibration is strongly influenced by the N-H rocking vibration.[51] The observed isotope effect on the C=N stretch and the N–H rock bands indicates that the Schiff base of the chromophore in SyHR is protonated in the unphotolyzed state. The observed C=N stretching frequency of SyHR (1639 cm^{-1}) was high compared to that of a typical chloride ion pump, HsHR (1635 cm^{-1})[44,45] and NpHR (1633 cm^{-1})[43] and is more similar to that of HsBR (1640 cm^{-1}).[32] In addition, the amplitude of the deuteration shift of the C=N stretch band was 16 cm^{-1} for SyHR, which is larger than that for HsHR (12 cm^{-1}) and NpHR (11 cm^{-1}) and is comparable to that for HsBR (16 cm^{-1}). It is known that a larger deuteration shift of the C=N stretching frequency means a stronger hydrogen bond

formation.[51] Thus these observations indicate that the hydrogen-bond strength of the Schiff base in SyHR is stronger than the chloride pumps.

Femtosecond time-resolved spectroscopic analysis of the retinal photoisomerization and the formation of early photointermediates

Because photointermediate states show characteristic absorption spectra, their formation and decay can be monitored by transient absorption changes in the visible region. To examine the photoisomerization process of the retinal chromophore, femtosecond time-resolved absorption measurements of SyHR were performed. Figures 7A-C show the time-resolved absorption spectra of SyHR at selected delay times, which were measured without salt, with 1 M NaCl or with 333 mM Na_2SO_4. Immediately after photoexcitation (0.1 ps), we observed a positive band in the 400-520 nm region and negative bands in the 530-600 nm and >650 nm regions. These transient bands are assigned to the $S_n \leftarrow S_1$ excited-state absorption (ESA), the ground-state bleaching (GSB) and the $S_1 \rightarrow S_0$ stimulated emission (SE). Subsequently, we observed decays of the ESA and SE bands in the picosecond time region. Concomitantly with the decay of these excited-state signals, a photoproduct absorption (PA) band appeared at around 630 nm, indicating the formation of SyHR having an isomerized retinal chromophore. After 100 ps, we observed no further spectral change within the time window of our measurement (1 ns).

To examine the photoisomerization dynamics more quantitatively, we performed global fitting analysis. Figures 7D-F show the temporal profiles of the transient absorption signals at selected wavelengths for each sample. These traces were successfully reproduced with a sum of five exponential functions that were convoluted with the instrumental response. The fitting results were overlaid on each trace (black curves in Figures 7D-F) and the obtained time constants and amplitudes are listed in Table 2 and Table S1 in Supporting information, respectively. The shortest lifetime component (τ_0, ~50 fs) was attributable to the blue-shift of the ESA band and the red-shift of the SE band, as previously reported for other rhodopsins.[52,53,54,55] According to these previous studies, we assigned the τ_0 component to the initial relaxation from the Franck-Condon state to the relaxed S_1 state. After these spectral shifts, the ESA and SE bands concomitantly decay with the time constants of τ_1, τ_2 and τ_3. Such multi-exponential behavior of the S_1 decay has been observed for other rhodopsins as well.[53,54,56,57] Although its origin is still under debate,[58] it has been proposed that some rhodopsins have structural heterogeneity in the ground state; multiple species that have slightly different environments around the chromophore are present in the sample.[59] These multiple species can be excited in parallel, and the generated S_1 states individually decay with different lifetimes reflecting different environments around the chromophore.

At the PA wavelengths, we observed a significant increase in the transient absorption

signal with a time constant of τ_1, and that time constant did not significantly change with the salt condition. These results indicate that the *trans-cis* photoisomerization of the retinal takes place with τ_1, irrespective of the salt conditions. In data measured with 1 M NaCl, we did not observe an increase of the PA signal with τ_2 and τ_3, indicating that the τ_1 process predominantly yields the photoproduct, and that the τ_2 and τ_3 processes do not significantly contribute to the photoproduct formation. These results suggest that τ_2 and τ_3 represent the S_1 lifetimes of the non-reactive sub-ensemble of SyHR, while τ_1 represents that of a reactive sub-ensemble which presumably has a chromophore environment more optimized for the isomerization. It should be noted that, under conditions without salt or with 333 mM Na_2SO_4, we observed an additional increase of components with τ_2 and τ_3 at the PA wavelength, suggesting that these processes may also generate the photoproduct. However, under these conditions, the PA amplitude is very small, and thus the time evolution of the PA amplitude is substantially obscured by the GSB and SE dynamics, which is not negligible at the PA wavelength. Therefore, currently we cannot conclude whether the τ_2 and τ_3 processes contribute to the photoproduct formation.

We observed a gradual blue-shift of the PA band by ~20 nm in the early picosecond time region (~10 ps) only in the presence of NaCl. This spectral change is attributable to the conversion from the J-intermediate to the K-intermediate, which has been well characterized for other rhodopsins.[54,57,60-62] The corresponding blue-shift was not recognized under the other salt conditions. This is probably because the quantum yield of the J-intermediate is low as described below, and the spectral change due to the J-to-K conversion is overwhelmed by the GSB and SE signals having larger amplitudes. Finally, the long-lived τ_4 component ($\tau_{4=\infty}$) is assigned to the K-intermediate whose lifetime is presumably in the order of microseconds.

It is worth noting that, irrespective of the salt condition, the amplitude of the PA signal is not as large as those of other rhodopsins such as HsBR and HsHR[58,63]. In fact, the ratio between the maximum amplitudes of the PA band at 100 ps and the GSB band at 0.1 ps, which provides an estimate of the quantum yield of the K intermediate (Φ_K), is significantly small, compared to the ratio observed for HsBR and HsHR. This indicates that Φ_K in SyHR is substantially lower than those in HsBR (Φ_K = 0.64) and HsHR (Φ_K = 0.34)[64-66]. SyHR has a chromophore environment that can accommodate both SO_4^{2-} and Cl^-. We consider that such unique environment might not be optimized for the isomerization of the retinal chromophore, giving rise to the low Φ_K value in SyHR. This argument is also consistent with the observation that the non-reactive components (τ_2 and τ_3) are predominant in the S_1 decay of SyHR.

Millisecond time-resolved spectroscopic analysis of the decay and formation of late photointermediates

Next, we investigated the photochemical reaction of SyHR in late photointermediates using millisecond flash-photolysis (Figure 8). Figures 8A-C show the transient difference absorption spectra of SyHR without salt, with 1 M NaCl and with 333 mM Na_2SO_4 over the spectral range of 400-710 nm in the millisecond time domain. Although absorption decreases and increases in the difference spectra were observed in all three conditions, no isosbestic point was present, indicating that multiple kinetic processes are involved in SyHR in this time domain. The light-induced absorption decreases at around 550 nm correspond to the bleaching of the original state, while the increases at around 460 nm and 600 nm were due to the formation of some photointermediates. Figures 8D-F show the time courses of the absorbance changes of SyHR at selected wavelengths. The decrease in absorption at shorter wavelengths (460-470 nm, denoted as $SyHR_{460\text{-}470\ nm}$) and the concomitant increase at longer wavelengths (600-630 nm, denoted as $SyHR_{600\text{-}630\ nm}$) imply reaction scheme 1 as follows;

$$SyHR \xrightarrow{h\nu} J \rightarrow K \rightarrow SyHR_{460\text{-}470\ nm} \rightarrow SyHR_{600\text{-}630\ nm} \rightarrow SyHR \qquad \text{(Scheme 1)}$$

To express the photoreaction more precisely, the time-dependent absorption changes were analyzed by global fitting according to the irreversible sequential model. For that analysis, we used the fitting function of the sum of three exponential terms, indicating the existence of three kinetically defined states in each state. As a result, the absorption spectra of the three states, designated as P_1−P_3, were calculated. The calculated spectra of the P_i species are shown in Figures 8 G, H and I. Note that the spectrum for P_0 represents the original SyHR with or without salts. P_1 has an absorption maximum at 490 nm in all conditions, which is tentatively assigned to the L-like intermediate, according to the absorption maximum and the sequence of intermediates observed in HRs. The component P_2 was produced by conversion from P_1 with the time constant τ_1 of 6.95 ms for SyHR without salt, 5.84 ms for SyHR with Cl^-, and 6.47 ms for SyHR with SO_4^{2-}. In this component, two peaks were observed (Figures 8 G, H and I). The state at around 580 nm is tentatively attributable to the O-like intermediate, according to the red-shifted absorption maximum and the analogy with HRs. Another state has a slightly longer absorption wavelength (510 nm) than does the L-like intermediate in P_1 (490 nm), suggesting the existence of a different intermediate from the L-like and O-like intermediates. Here we tentatively assigned that state as an N-like intermediate. In NpHR, the N and O intermediates are, respectively, the Cl^--bound and Cl^--unbound states at the CP half channel. They are in quasi-equilibrium and thus their molar ratio is changed depending on the salt concentration. To verify this, we carried out flash-photolysis measurements at several salt concentrations. In the case of Cl^- (shown in Figure 8J), the absorptions of the N-like and O-like intermediates increase

and decrease together with the increase in NaCl concentration, respectively. This result suggests that the tentatively assigned N-like and O-like intermediates are similar to the Cl^--bound and Cl^--unbound states of NpHR,[67] respectively. Similarly, in the case of SO_4^{2-}, the ratio of the N-like/O-like intermediates is likely to increase in a Na_2SO_4 concentration-dependent manner (Figure 8K), suggesting the movement of SO_4^{2-} at the P_2 state. During the transition from the P_2 to the P_3 state, a spectral red shift from 490 to 580 nm due to the accumulation of the red-shifted O-like intermediate was clearly observed except in SyHR with Cl^-. The time constant τ_2 was estimated to be 19.0 ms for SyHR without salt, 17.7 ms for SyHR with Cl^- and 19.0 ms for SyHR with SO_4^{2-}. The λ_{max} of the P_3 state of SyHR with Cl^- was almost the same as that of the original (unphotolyzed) state P_0, suggesting that the P_3 state of SyHR with Cl^- contains an intermediate named SyHR′ that has the same λ_{max} as the original SyHR. P_3 was then converted to the original P_0 with the time constant τ_3 of 153 ms for SyHR without salt, 40.0 ms for SyHR with Cl^- and 664 ms for SyHR with SO_4^{2-}, and finally the photocycle was completed. On the basis of these results, we propose a putative model for the photocycle of SyHR with or without substrate ions (Figure 9).

DISCUSSION

Anion binding site in SyHR

To summarize our results, the photobiological and photochemical properties of anion transporting rhodopsins, SyHR, MrHR, HsHR and NpHR, are listed in Table 1. HsHR and NpHR are able to transport monoatomic monovalent anions (practically halide ions) and polyatomic monovalent anions (NO_3^- and SCN^-), but not the polyatomic divalent anion, SO_4^{2-}. Earlier studies of HsHR and NpHR revealed that their Cl^- binding site is located in the vicinity of the protonated Schiff base. In the case of NpHR, the binding site is composed of 10 amino acids (Val77, Ser78, Ser81, Arg123, Thr126, Trp127, Ser130, Thr131, Asp252 and Lys256) (Figure 10A).[10] The Cl^- binding site is located near Thr126, which corresponds to the primary counter ion for the protonated Schiff base, Asp85, in HsBR. The Cl^- forms an electric quadrupolar complex together with the protonated Schiff base, Arg123 and Asp252, and is also stabilized by the three water molecules (W502, W503 and W504).[10] On the other hand, the corresponding residues in SyHR are Ile45, Ala46, Leu49, Arg71, Thr74, Trp75, Ser78, Thr79, Asp201 and Lys205. Among them, one of the critical residues for anion binding in HRs, Thr74 in SyHR, is conserved, whereas the number of OH-group bearing residues (Ser and Thr) in SyHR is less than those in NpHR (i.e., Ser78 and Ser81 in NpHR are replaced by non-polar residues, Ala and Leu), indicating less hydrophilicity in the binding site of SyHR. In SyHR, the binding constant K_d for Cl^- is 0.112 mM, which is ca. 20-times stronger than other anion pumps, HsHR, NpHR and MrHR,[11,12,19] and more than 500-times stronger than FR.[68] This indicates that

the bound Cl^- is strongly stabilized in the binding site probably.

The most remarkable phenomenon is that SyHR transports a polyatomic divalent anion SO_4^{2-} (ionic radius 2.42 Å), which is significantly larger than Cl^- (ionic radius 1.80 Å)[69] (Figure 2). The absorption spectra in Figure 3A indicate that SyHR binds SO_4^{2-} together with the spectral red shift, which is opposite the case of Cl^- binding. The absorption maximum of microbial rhodopsins corresponds to its lowest π-π* excitation energy. In the electric ground state, a positive charge is localized mainly on the Schiff base nitrogen, and upon excitation, it shifts toward the β-ionone ring (Figure 10A).[70,71] The binding of Cl^- to the protonated Schiff base nitrogen in SyHR leads to a decrease in the energy of the ground state, resulting in a spectral blue shift as occurs in NpHR,[16] while the binding of SO_4^{2-} has to establish an increase in the energy of the ground state or a decrease in the energy of the excited state. The spectral red shift upon anion binding is also seen in the anion pumps HsHR and MrHR, and in the phototaxis sensor *Salinibacter ruber* sensory rhodopsin I (SrSRI). In the case of HsHR, Cl^- is bound to the vicinity of the protein near the protonated Schiff base as occurs in NpHR.[9,10] On the other hand, in the case of SrSRI, Cl^- is bound in the vicinity of a β-ionone ring of the retinal chromophore, which induces the destabilization of the π-conjugation system.[72] Thus there are roughly two possibilities regarding the SO_4^{2-} binding site in SyHR (i.e., the Schiff base vs the β-ionone ring). In the presence of SO_4^{2-}, a spectral blue shift was observed upon the addition of Cl^- and the λ_{max} reached 536 nm (Figures 4A, B and E), which is identical to that in the presence of only Cl^- (Figures 3A and G). This result suggests that SO_4^{2-} is replaced by Cl^- and thus SO_4^{2-} shares the same binding site with Cl^-. In almost all of the microbial ion-pumping rhodopsins, the transport substrate ions (H^+, Cl^-, Na^+) pass through the protonated Schiff base region rather than the vicinity of the β-ionone ring of the retinal chromophore. Therefore, it is reasonable to conclude that SO_4^{2-} is bound to the vicinity around the protonated Schiff base in SyHR. The binding constant K_d for SO_4^{2-} in SyHR was estimated to be 5.81 mM, which is ca. 40-times weaker than that for Cl^- but is in the same order with those for Cl^- in HsHR, NpHR and MrHR (Table 1). Because of the SO_4^{2-} binding, the electric quadrupolar complex structure (Figure 10) can be greatly changed to compensate for the residual negative charge. Another positive charge is needed based on the conventional model. Thus, it is likely that structural rearrangement of a positively-charged side chain and/or protonation to an amino acid residue take place near the chromophore. Furthermore, the ion hydrogen-bonded to the protonated Schiff base can interact with the polyene chain at another negatively charged oxygen atom (See Figure S1 in Supporting information). We suppose that such a multiple interaction of SO_4^{2-} with the chromophore led to the shift of absorption maximum opposite to the shift induced by other anions.

Anion transport mechanism in SyHR

In microbial rhodopsins, upon the formation and decay of the early photointermediates J and K, the retinal chromophore is isomerized from all-*trans* to 13-*cis*, while the substrate ions including H^+, Na^+ and Cl^-, stay at the initial binding site(s). Therefore, we focused on events that occur after the decay of the K intermediate of SyHR. As a reference, the photocycle of the Cl^--bound NpHR is described in the following scheme;

$$\text{NpHR} \xrightarrow{h\nu} (\text{K}) \rightarrow \text{L}_1 \rightarrow \text{L}_2 \rightarrow \text{N} \rightleftarrows \text{O} \rightleftarrows \text{NpHR'} \rightarrow \text{NpHR} \quad \text{(Scheme 2)}$$

In SyHR, the L-, N- and O-like intermediates were observed as well as NpHR (Figure 8). Both in the presence of Cl^- or SO_4^{2-}, the L-like intermediate appeared as the photoproduct P_1, as shown in Figures 8H and I. We noticed that the spectral width of the L-like intermediate seems to be wide. Therefore, we speculate that the L-like intermediate may be a multiple state. The anion concentration dependence in P_2 absorption spectra indicates that SyHR releases and takes up cognate anions (Cl^- and SO_4^{2-}) upon the formation and decay of the O-like intermediate, respectively (Figure 9), which is basically the same as the scheme of NpHR (Scheme 2). The Cl^- binding affinity corresponding to the Cl^- releasing process was roughly estimated to be lower than 100 mM, as judged by the transition of the molar ratio of the N-like and O-like intermediates (Figure 8J). The O-like intermediate decays with the rebinding of the anions to the initial binding site as shown in the P_3 absorption spectra (Figures 8H and I). However, this step is highly affected by the anions as shown in the time constant τ_3 (40.0 ms for Cl^- and 664 ms for SO_4^{2-}). In the presence of Cl^-, the O-like intermediate is converted to SyHR', which also occurs in NpHR.[67] On the other hand, in the presence of SO_4^{2-}, the SyHR' intermediate does not need to be considered in the analysis (Figure 9B). These results suggest that the anion uptake processes are different from the cases for Cl^- and SO_4^{2-}.

Compared to the amino acid sequences of the CP half channel in SyHR and NpHR, SyHR has 13 basic amino acid residues, Arg and Lys, more than 7 of those in NpHR. Especially from the 5th to 6th (E to F) helices, 7 of the 13 residues are involved in the CP half channel in SyHR while 2 of the 7 residues are involved in NpHR. In the homologous protein MrHR, 10 basic residues are seen and 6 of them are distributed in the CP side of the E and F helices. However, 2 of the 7 residues are not aligned with the basic residues in SyHR. Therefore, we speculate that such a positively charged cluster may be one of the mechanisms for the SO_4^{2-} transportation in SyHR and the distribution of the basic residues may be optimized for the SO_4^{2-} transporter because the similar cyanobacterial Cl^- pump MrHR does not transport SO_4^{2-}.[19] In addition, water molecules presumably play important roles for anion transport as they do in other membrane-embedded ion transporters. The CP half channel of NpHR is hydrophobic and

only one water molecule is seen near Thr218 in the crystal structure.[10] The CP half channel of SyHR is even less polar and Thr218 in NpHR is replaced by His167. The crystal structure of the N-intermediate of NpHR suggested that the number of water molecules is increased upon structural change from one water molecule in the initial state.[15] Moreover, time-resolved Fourier transformed infrared (FT-IR) spectroscopy revealed that the Cl^- transport is accompanied by the dynamic rearrangement of the hydrogen bond network of internal water molecules, which is expected to facilitate Cl^- transport in the N-intermediate of NpHR.[73] Therefore, we speculate that the transient influx of water molecules and the rearrangement of hydrogen bonds are also important for the Cl^- and SO_4^{2-} transporting functions of SyHR. On the basis of the hypothesis, a putative model for the anion transportation in SyHR is proposed, as shown in Figures 9 and 10B. The physiological significance of SO_4^{2-} transport including the curious issue whether SyHR works as an active (pump) or a passive (channel) ion transporter is our next focus and it would be examined by electrophysiological experiments. Of note, it is well-known that the pK_a of the functional groups is dramatically altered upon interaction with protein moiety. For example, the pK_a of Asp96 in HsBR has been reported as above 11.[20] Thus, there is a possibility that the sulfate anion exists as a monovalent $HSO4^-$ anion inside the protein. The anionic state in SyHR is also our next research focus.

In conclusion, we reported here a novel ion transporting rhodopsin, SyHR, which transports not only a monoatomic monovalent anion (Cl^-), but also a polyatomic divalent anion (SO_4^{2-}). As far as we know, SyHR is the first light-driven SO_4^{2-} transporter in nature. Thus, SyHR opens new avenues to understand and utilize divalent anion transporters.

AUTHOR INFORMATION

Corresponding Author

sudo@okayama-u.ac.jp

Notes

The authors declare no competing financial interests.

ACKNOWLEDGEMENTS

The authors thank Dr. Satoshi Takeuchi (Molecular Spectroscopy Laboratory, RIKEN) for assistance with the femtosecond time-resolved spectroscopy and fruitful discussions of the results. This research was supported by grants from the Japanese Ministry of Education, Culture, Sports, Science, and Technology (MEXT) to S.Y. (JP15H02800), T.Ts. (JP15K18519) and Y.S. (JP15H04363, JP15H00878 and JP25104005), by the Interdisciplinary Collaborative Research Program of the Atmosphere and Ocean Research Institute, the University of Tokyo to S.Y. and Y.S., and by the Uehara Memorial Foundation to Y.S. This research was also financially

supported by a grant-in-aid for scientific research on the innovative area (no. 2503, soft molecular systems) to T.Ta., Y. M and Y.S. (JP25104005 and JP25104006).

REFERENCES

(1) Ernst, O. P.; Lodowski, D. T.; Elstner, M.; Hegemann, P.; Brown, L. S.; Kandori, H. *Chem Rev* **2014**, *114*, 126.

(2) Inoue, K.; Tsukamoto, T.; Sudo, Y. *Biochim Biophys Acta* **2014**, *1837*, 562.

(3) Yoshizawa, S.; Kawanabe, A.; Ito, H.; Kandori, H.; Kogure, K. *Environ Microbiol* **2012**, *14*, 1240.

(4) Martinez, A.; Bradley, A. S.; Waldbauer, J. R.; Summons, R. E.; DeLong, E. F. *Proc Natl Acad Sci U S A* **2007**, *104*, 5590.

(5) Oesterhelt, D.; Stoeckenius, W. *Nat New Biol* **1971**, *233*, 149.

(6) Matsuno-Yagi, A.; Mukohata, Y. *Arch Biochem Biophys* **1980**, *199*, 297.

(7) Bivin, D. B.; Stoeckenius, W. *J Gen Microbiol* **1986**, *132*, 2167.

(8) Varo, G.; Brown, L. S.; Sasaki, J.; Kandori, H.; Maeda, A.; Needleman, R.; Lanyi, J. K. *Biochemistry* **1995**, *34*, 14490.

(9) Kolbe, M.; Besir, H.; Essen, L. O.; Oesterhelt, D. *Science* **2000**, *288*, 1390.

(10) Kouyama, T.; Kanada, S.; Takeguchi, Y.; Narusawa, A.; Murakami, M.; Ihara, K. *J Mol Biol* **2010**, *396*, 564.

(11) Steiner, M.; Oesterhelt, D.; Ariki, M.; Lanyi, J. K. *J Biol Chem* **1984**, *259*, 2179.

(12) Scharf, B.; Engelhard, M. *Biochemistry* **1994**, *33*, 6387.

(13) Hackmann, C.; Guijarro, J.; Chizhov, I.; Engelhard, M.; Rodig, C.; Siebert, F. *Biophys J* **2001**, *81*, 394.

(14) Hasegawa, C.; Kikukawa, T.; Miyauchi, S.; Seki, A.; Sudo, Y.; Kubo, M.; Demura, M.; Kamo, N. *Photochem Photobiol* **2007**, *83*, 293.

(15) Kouyama, T.; Kawaguchi, H.; Nakanishi, T.; Kubo, H.; Murakami, M. *Biophys J* **2015**, *108*, 2680.

(16) Sato, M.; Kanamori, T.; Kamo, N.; Demura, M.; Nitta, K. *Biochemistry* **2002**, *41*, 2452.

(17) Rippka, R.; Deruelles, J.; Waterbury, J. B.; Herdman, M.; Stanier, R. Y. *J Gen Microbiol* **1979**, *111*, 1.

(18) Mueller, M. H.; Weingartner, R.; Alewell, C. *Hydrol Earth Syst Sc* **2013**, *17*, 1661.

(19) Hasemi, T.; Kikukawa, T.; Kamo, N.; Demura, M. *J Biol Chem* **2016**, *291*, 355.

(20) Balashov, S. P. *Biochim Biophys Acta* **2000**, *1460*, 75.

(21) Kandori, H.; Kinoshita, N.; Yamazaki, Y.; Maeda, A.; Shichida, Y.; Needleman, R.; Lanyi, J. K.; Bizounok, M.; Herzfeld, J.; Raap, J.; Lugtenburg, J. *Biochemistry* **1999**,

38, 9676.

(22) Tsukamoto, T.; Inoue, K.; Kandori, H.; Sudo, Y. *J Biol Chem* **2013**, *288*, 21581.

(23) Kitajima-Ihara, T.; Furutani, Y.; Suzuki, D.; Ihara, K.; Kandori, H.; Homma, M.; Sudo, Y. *J Biol Chem* **2008**, *283*, 23533.

(24) Tsukamoto, T.; Kikukawa, T.; Kurata, T.; Jung, K. H.; Kamo, N.; Demura, M. *FEBS Lett* **2013**, *587*, 322.

(25) Kolthoff, I. M. In *Treatise on Analytical Chemistry*; Kolthoff, I. M., Elving, P. J. Eds.; Interscience Encyclopedia, Inc., New York, **1959**.

(26) Kamo, N.; Muratsugu, M.; Hongoh, R.; Kobatake, Y. *J Membrane Biol* **1979**, *49*, 105.

(27) Yamashita, Y.; Kikukawa, T.; Tsukamoto, T.; Kamiya, M.; Aizawa, T.; Kawano, K.; Miyauchi, S.; Kamo, N.; Demura, M. *Biochim Biophys Acta* **2011**, *1808*, 2905.

(28) Casadio, R.; Gutowitz, H.; Mowery, P.; Taylor, M.; Stoeckenius, W. *Biochim Biophys Acta* **1980**, *590*, 13.

(29) Sineshchekov, O. A.; Trivedi, V. D.; Sasaki, J.; Spudich, J. L. *J Biol Chem* **2005**, *280*, 14663.

(30) Yoshitsugu, M.; Shibata, M.; Ikeda, D.; Furutani, Y.; Kandori, H. *Angew Chem Int Ed Engl* **2008**, *47*, 3923.

(31) Marti, T.; Rosselet, S. J.; Otto, H.; Heyn, M. P.; Khorana, H. G. *J Biol Chem* **1991**, *266*, 18674.

(32) Smith, S. O., Braiman, M. S., Myers, A. B., Pardoen, J. A., Courtin, J. M. L., Winkel, C., Lugtenburg, J., and Mathies, R. A. *J. Am. Chem. Soc.* **1987**, *109*, 3108.

(33) Furutani, Y.; Sudo, Y.; Wada, A.; Ito, M.; Shimono, K.; Kamo, N.; Kandori, H. *Biochemistry* **2006**, *45*, 11836.

(34) Smith, S. O.; Pardoen, J. A.; Lugtenburg, J.; Mathies, R. A. *J Phys Chem* **1987**, *91*, 804.

(35) Curry, B.; Broek, A.; Lugtenburg, J.; Mathies, R. *J. Am. Chem. Soc.* **1982**, *104*, 5274.

(36) Mathies, R. A. In *Biological Applications of Raman Spectroscopy*; John & Wiley Sons, Inc., New York, **1987**.

(37) Aton, B.; Doukas, A. G.; Callender, R. H.; Becher, B.; Ebrey, T. G. *Biochemistry* **1977**, *16*, 2995.

(38) Smith, S. O.; Lugtenburg, J.; Mathies, R. A. *J Membr Biol* **1985**, *85*, 95.

(39) Krebs, R. A.; Dunmire, D.; Partha, R.; Braiman, M. S. *J Phys Chem B* **2003**, *107*, 7877.

(40) Miranda, M. R.; Choi, A. R.; Shi, L.; Bezerra, A. G., Jr.; Jung, K. H.; Brown, L. S. *Biophys J* **2009**, *96*, 1471.

(41) Furutani, Y.; Bezerra, A. G., Jr.; Waschuk, S.; Sumii, M.; Brown, L. S.; Kandori, H.

Biochemistry **2004**, *43*, 9636.

(42) Kralj, J. M.; Bergo, V. B.; Amsden, J. J.; Spudich, E. N.; Spudich, J. L.; Rothschild, K. J. *Biochemistry* **2008**, *47*, 3447.

(43) Gerscher, S.; Mylrajan, M.; Hildebrandt, P.; Baron, M. H.; Muller, R.; Engelhard, M. *Biochemistry* **1997**, *36*, 11012.

(44) Maeda, A.; Ogurusu, T.; Yoshizawa, T.; Kitagawa, T. *Biochemistry* **1985**, *24*, 2517.

(45) Ames, J. B.; Raap, J.; Lugtenburg, J.; Mathies, R. A. *Biochemistry* **1992**, *31*, 12546.

(46) Fodor, S. P.; Gebhard, R.; Lugtenburg, J.; Bogomolni, R. A.; Mathies, R. A. *J Biol Chem* **1989**, *264*, 18280.

(47) Gellini, C.; Luttenberg, B.; Sydor, J.; Engelhard, M.; Hildebrandt, P. *FEBS Lett* **2000**, *472*, 263.

(48) Mironova, O. S.; Efremov, R. G.; Person, B.; Heberle, J.; Budyak, I. L.; Buldt, G.; Schlesinger, R. *FEBS Lett* **2005**, *579*, 3147.

(49) Nack, M.; Radu, I.; Bamann, C.; Bamberg, E.; Heberle, J. *FEBS Lett* **2009**, *583*, 3676.

(50) Yi, A.; Mamaeva, N.; Li, H.; Spudich, J. L.; Rothschild, K. J. *Biochemistry* **2016**, *55*, 2371.

(51) Baasov, T.; Friedman, N.; Sheves, M. *Biochemistry* **1987**, *26*, 3210.

(52) Mathies, R. A.; Brito Cruz, C. H.; Pollard, W. T.; Shank, C. V. *Science* **1988**, *240*, 777.

(53) Nakamura, T.; Takeuchi, S.; Shibata, M.; Demura, M.; Kandori, H.; Tahara, T. *J Phys Chem B* **2008**, *112*, 12795.

(54) Sudo, Y.; Mizuno, M.; Wei, Z.; Takeuchi, S.; Tahara, T.; Mizutani, Y. *J Phys Chem B* **2014**, *118*, 1510.

(55) Dobler, J.; Zinth, W.; Kaiser, W.; Oesterhelt, D. *Chem Phys Lett* **1988**, *144*, 215.

(56) Lenz, M. O.; Huber, R.; Schmidt, B.; Gilch, P.; Kalmbach, R.; Engelhard, M.; Wachtveitl, J. *Biophys J* **2006**, *91*, 255.

(57) Tahara, S.; Takeuchi, S.; Abe-Yoshizumi, R.; Inoue, K.; Ohtani, H.; Kandori, H.; Tahara, T. *J Phys Chem Lett* **2015**, *6*, 4481.

(58) Iyer, E. S. S.; Misra, R.; Maity, A.; Liubashevski, O.; Sudo, Y.; Sheves, M.; Ruhman, S. *J Am Chem Soc* **2016**, *138*, 12401.

(59) Gai, F.; Hasson, K. C.; McDonald, J. C.; Anfinrud, P. A. *Science* **1998**, *279*, 1886.

(60) Nuss, M. C.; Zinth, W.; Kaiser, W.; Kolling, E.; Oesterhelt, D. *Chem Phys Lett* **1985**, *117*, 1.

(61) Polland, H. J.; Franz, M. A.; Zinth, W.; Kaiser, W.; Kolling, E.; Oesterhelt, D. *Biophys J* **1986**, *49*, 651.

(62) Lutz, I.; Sieg, A.; Wegener, A. A.; Engelhard, M.; Boche, I.; Otsuka, M.; Oesterhelt,

D.; Wachtveitl, J.; Zinth, W. *Proc Natl Acad Sci U S A* **2001**, *98*, 962.

(63) Arlt, T.; Schmidt, S.; Zinth, W.; Haupts, U.; Oesterhelt, D. *Chem Phys Lett* **1995**, *241*, 559.

(64) Govindjee, R.; Balashov, S. P.; Ebrey, T. G. *Biophys J* **1990**, *58*, 597.

(65) Tittor, J.; Oesterhelt, D. *FEBS Letters* **1990**, *263*, 269.

(66) Oesterhelt, D.; Hegemann, P.; Tittor, J. *Embo Journal* **1985**, *4*, 2351.

(67) Kikukawa, T.; Kusakabe, C.; Kokubo, A.; Tsukamoto, T.; Kamiya, M.; Aizawa, T.; Ihara, K.; Kamo, N.; Demura, M. *Biochim Biophys Acta* **2015**, *1847*, 748.

(68) Inoue, K.; Koua, F. H.; Kato, Y.; Abe-Yoshizumi, R.; Kandori, H. *J Phys Chem B* **2014**, *118*, 11190.

(69) Marcus, Y. *Chem Rev* **1988**, *88*, 1475.

(70) Nielsen, M. B. *Chem Soc Rev* **2009**, *38*, 913.

(71) Sudo, Y.; Okazaki, A.; Ono, H.; Yagasaki, J.; Sugo, S.; Kamiya, M.; Reissig, L.; Inoue, K.; Ihara, K.; Kandori, H.; Takagi, S.; Hayashi, S. *J Biol Chem* **2013**, *288*, 20624.

(72) Suzuki, D.; Furutani, Y.; Inoue, K.; Kikukawa, T.; Sakai, M.; Fujii, M.; Kandori, H.; Homma, M.; Sudo, Y. *J Mol Biol* **2009**, *392*, 48.

(73) Furutani, Y.; Fujiwara, K.; Kimura, T.; Kikukawa, T.; Demura, M.; Kandori, H. *J Phys Chem Lett* **2012**, *3*, 2964.

(74) Kralj, J. M.; Spudich, E. N.; Spudich, J. L.; Rothschild, K. J. *J Phys Chem B* **2008**, *112*, 11770.

(75) Ogurusu, T.; Maeda, A.; Sasaki, N.; Yoshizawa, T. *Biochim Biophys Acta* **1982**, *682*, 446.

FIGURE LEGENDS

Figure 1. Phylogenetic properties of the newly identified microbial rhodopsin SyHR

(A) Phylogenetic tree of microbial rhodopsins. Three proton pumps, bacteriorhodopsin from the archaeon *Halobacterium salinarum* R1 (HsBR), proteorhodopsin from a marine bacterioplankton (PR) and thermophilic rhodopsin from the eubacterum *Thermus thermophilus* JL-18 (TR), and 3 anion pumps, halorhodopsins from the archaea *Halobacterium salinarum* R1 (HsHR) and *Natronomonas pharaonis* DSM2160 (NpHR) and from the eubacterium *Mastigocladopsis repens* PCC 10914 (MrHR), are mapped on the tree with *Synechocystis* halorhodopsin (SyHR) and sensory rhodopsins (HsSRI, SrSRI, NpSRII and HsSRII) using ClustalW (http://clustalw.ddbj.nig.ac.jp/). (B) Alignment of critical amino acids of microbial ion pumping rhodopsins created using ClustalW. SyHR has a TSD motif (Thr74, Ser78 and Asp85) as does MrHR, which is replaced by a TSA sequence in the anion pumps HsHR and NpHR, and

by a DTD sequence in the proton pumps HsBR, PR and TR. On the basis of that background, SyHR is assumed to be a light-drive anion pump. (C) Putative secondary structure of SyHR predicted by a protein secondary structure prediction server JPred4 (http://www.compbio.dundee.ac.uk/jpred/), which automatically searches proteins sharing high sequential similarities from the Protein Data Bank as a reference for a more accurate prediction.

Figure 2. Anion pumping activity of SyHR

Light-induced pH changes of *E. coli* cell suspensions expressing SyHR in solutions containing: (A) monoatomic anions 100 mM NaCl, 100 mM NaBr, 100 mM NaI or 100 mM KCl, and (B) polyatomic anions 100 mM $NaNO_3$ or 100 mM Na_2SO_4, were observed in the absence (grey broken lines) or presence (black solid lines) of the protonophore CCCP (10 μM), or in the presence of 10 μM CCCP and 20 mM TPP^+ (black broken lines). Each cell suspension was placed in the dark and was illuminated using a 300 W xenon lamp with a 520 nm band-pass filter for 3 min at 25°C. Light-induced pH changes of *E. coli* cell suspensions harboring the pET22b vector are shown as a negative control. (C) Ionic states of sulfate under varying pH. There are two deprotonated groups with two different pKa values. In this report, we performed the experiments at pHs ranging from 5 to 7.

Figure 3. Effects of anions on UV-Visible absorption spectra and the chromophore configuration of SyHR

(A) UV-Visible absorption spectra of SyHR in the presence or absence of anions. (B) HPLC patterns of the retinal oxime in the presence or absence of anions. Extraction of retinal oxime from purified SyHR was carried out with hexane after denaturation by methanol and 500 mM hydroxylamine at 4°C. (C) UV-Vis spectral changes of SyHR following the addition of NaCl and (D) their difference spectra. (E) UV-Vis spectral changes of SyHR following the addition of Na_2SO_4, and (F) their difference spectra. (G) Absorption changes at 592 nm in the difference spectra plotted against the salt concentrations. The data were fitted by the Hill equation (solid lines) to estimate the affinity of the anions. The fitting parameter, ΔA_{max}, was set as 1. All titration experiments were performed at room temperature (approx. 25°C).

Figure 4. Competition experiments of two anion species, Cl^- and SO_4^{2-}

(A) NaCl-dependent changes of UV-Visible absorption spectra of SyHR in the presence of 1 M Na_2SO_4, and (B) their difference spectra. (C) Na_2SO_4-dependent changes of UV-Visible absorption spectra of SyHR in the presence of 1 M NaCl, and (D) their difference spectra. (E) Absorption changes at 594 nm in the difference spectra plotted against the salt concentrations. The data were fitted by the Hill equation (solid lines) to estimate the affinity of anions. The

experiments were performed at room temperature (approx. 25°C).

Figure 5. Estimation of pK_a of the charged residues in SyHR

UV-Visible spectra of SyHR over a wide pH range of 4-11 without salt (A) or with 1 M NaCl (C) or 0.333 M Na_2SO_4 (E). From analogy with other microbial rhodopsins such as HsBR and HsHR, the spectral blue shifts to around 400 nm observed for all conditions presumably correspond to the formation of the deprotonated Schiff base. Panels B, D and F show the difference spectra of SyHR without salt (B) or with 1 M NaCl (D) or 0.333 M Na_2SO_4 (F). (G) Absorption changes in the difference spectra at 409 nm (left axis, for the sample in the absence of salt or in the presence of 0.333 M Na_2SO_4) and at 397 nm (right axis, for the sample in the presence of 1 M NaCl) plotted against the pH values and data were fitted by the Henderson-Hasselbalch equation with a single pK_a value (solid line). pK_a values were estimated as approximately 9.48 for no salt, 10.6 for NaCl and 8.92 for Na_2SO_4. The experiments were performed at room temperature (approx. 25 °C).

Figure 6. Resonance Raman spectroscopic analysis of the retinal chromophore in SyHR

(A) Resonance Raman spectra of the retinal chromophore in SyHR without salt (top), with 1 M NaCl (middle) and with 333 mM SO_4 (bottom). Excitation wavelength was 532 nm. Red and blue traces represent the resonance Raman spectra measured in H_2O buffer and D_2O buffer, respectively. The experiments were performed at room temperature (approx. 25°C). An asterisk represents a band due to the vibration of the sulfate ion. (B) Plot of the C=C stretching frequency against the absorption maximum wavelength for 14 types of retinal proteins (1: Blue PR,[74] 2: Green PR,[74] 3: Neurospora rhodopsin,[41] 4: Gloeobacter rhodopsin,[40] 5: PR,[39] 6: HsBR,[38] 7: NO_3^- bound HsHR,[44] 8, 9: Cl^- bound HsHR,[44,45] 10: Cl^- bound NpHR,[43] 11: anion-depleted NpHR,[43] 12: *Halobacterium salinarum* sensory rhodopsin II,[48] 13: *Natronomonas pharaonis* sensory rhodopsin II,[47] and 14: *Halobacterium salinarum* sensory rhodopsin I[46]) and SyHR with or without salt. Purple, cyan, green and red circles are plots for proton pumps, anion pumps, sensors and SyHR, respectively. The black line is the best-fit with a linear function for the data reported previously.

Figure 7. Femtosecond time-resolved absorption spectroscopic analysis of excited state dynamics and early photointermediates in SyHR

(A-C) Femtosecond time-resolved absorption spectra of SyHR measured without salt, with 1 M NaCl or with 333 mM Na_2SO_4. The experiments were performed at room temperature (approx. 25°C). The wavelength region masked in white is distorted by the scattering of the pump pulse. (D-F) Temporal profiles of the transient absorption signals at selected wavelengths. The black

solid curves represent the best fit to the data. Note that the horizontal scale is changed from linear to logarithmic after 3 ps. The time region at around 0 ps masked in white is distorted by coherent artifact.

Figure 8. Millisecond time-resolved absorption spectroscopic analysis of late photointermediates in SyHR

Flash-induced difference spectra of SyHR without salts (A) or with 1 M NaCl (B) or 0.333 M Na_2SO_4 (C) over a spectral range from 400 to 710 nm and a time range from 0.7 to 1028 ms. The transient absorption change of the purified SyHR at 460, 540 or 550 and 620 nm without salts (D) or with 1 M NaCl (E) or 0.333 M Na_2SO_4 (F). The data were fitted by 3 time constants, τ_1, τ_2 andτ_3 (gray lines). The calculated absorption of 3 intermediates, P_1, P_2 and P_3 and an initial state P_0, without salt (G) or with 1 M NaCl (H) or 333 mM Na_2SO_4 (I). (J, K) Cl^-- and SO_4^{2-}-dependent spectral changes in the P_2 state. The experiments were performed at 25°C.

Figure 9. Putative model for the photoreaction kinetics of SyHR with the timing of anion movements

Based of the results of this study together with other findings, we propose photocycle models for SyHR without anions (A) or with Cl^- (B) or SO_4^{2-} (C).

Figure 10. Schematic of the putative anion transport mechanism in SyHR

(A) Putative anion binding site in the unphotolyzed (original) state of SyHR illustrated by reference to the crystal structure of NpHR (PDB ID 3A7K).[10] The numbers of amino acid residues correspond to NpHR and SyHR (denoted in parenthesis). The residues colored red and blue are positively or negatively charged ones and OH-group bearing ones, respectively. Three water molecules observed in the crystal structure of NpHR are also illustrated. (B) Anion transport model of SyHR based on the results obtained in this study. (i)-(iii) indicate the sequences of anion transportation.

Table 1. Photobiological and photochemical properties of SyHR compared with other anion pumping rhodopsins, MrHR, HsHR and NpHR. n.d. indicates "not determined".

Opsin type	**Substrates**	**Absorption maximum [nm]**	**Retinal conformer**	**Affinity of anions [mM]**	**p*Ka* of the Schiff base**	**Refs.**
SyHR	Cl^-, Br^-, SO_4^{2-}	542 (w/o salt), 536 (Cl^-), 556(SO_4^{2-})	all-*trans* (94.1 %)	0.112 (Cl^-), 5.81 (SO_4^{2-})	9.48 (w/o salt), 10.6 (Cl^-), 8.92 (SO_4^{2-})	This study
MrHR	Cl^-, Br^-	506 (w/o salt) 537 (Cl^-)	all-*trans* (> 98 %)	1.99 (Cl^-)	n.d.	[19]
HsHR	Cl^-, Br^-, NO_3^-	565 (w/o salt) 578 (Cl^-)	Light-adapted : all-*trans* (83%), Dark-adapted : all-*trans* (48%),	10 (Cl^-)	7.4 (w/o salt), 8.9 (Cl^-)	[8,11,75]
NpHR	Cl^-, Br^-, NO_3^-	600 (w/o salt) 578 (Cl^-)	Light-adapted : all-*trans* (77%), Dark-adapted : all-*trans* (83%),	2 (Cl^-)	8.5(w/o salt), 9.6 (Cl^-)	8, 12

Table 2. Time constants and assignments.

	No salt	1 M NaCl	333 m M Na_2SO_4	Assignments
τ_0 /ps	0.05 ± 0.01	0.04 ± 0.02	0.06 ± 0.05	FC → relaxed S_1
τ_1 /ps	0.45 ± 0.05	0.43 ± 0.08	0.38 ± 0.04	Reactive S_1 → J intermediate
τ_2 /ps	2.0 ± 0.2	1.4 ± 0.2	2.7 ± 0.2	Non-reactive S_1 → original S_0
τ_3 /ps	14 ± 5	4.5 ± 0.3	16 ± 1	Non-reactive S_1 → original S_0
τ_4 /ps	> 1000	> 1000	> 1000	K intermediate decay

Figure1

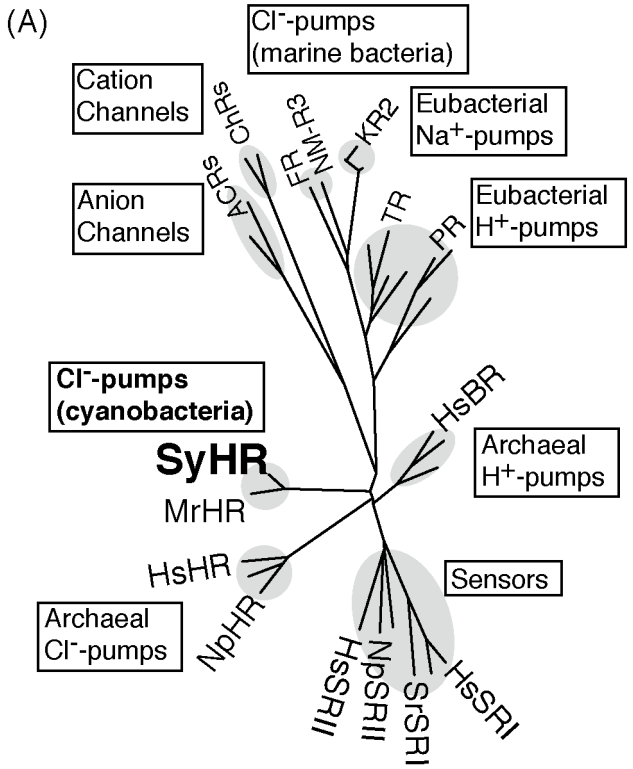

(B)

	No. in BR	82	85	89	96	194	204	212	216
	No. in SyHR	71	74	78	85	183	193	201	205
H^+ pump	HsBR	R	**D**	**T**	**D**	E	E	D	K
	TR	R	**D**	**T**	**E**	W	A	D	K
Cl^- pump	HsHR	R	**T**	**S**	**A**	E	T	D	K
	NpHR	R	**T**	**S**	**A**	E	T	D	K
	FR	R	**N**	**T**	**Q**	L	R	D	K
	NM-R3	R	**N**	**T**	**Q**	F	R	D	K
	MrHR	R	**T**	**S**	**D**	E	E	D	K
	SyHR	R	**T**	**S**	**D**	T	E	D	K

(C)

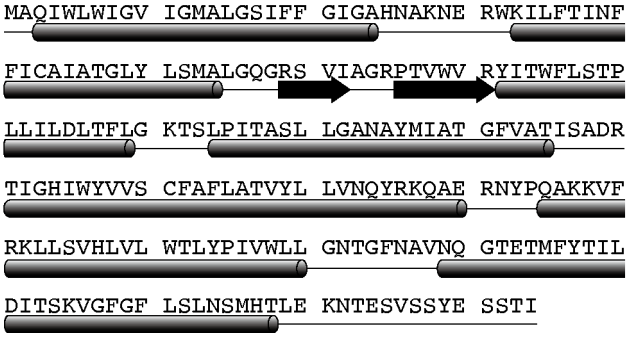

Figure2

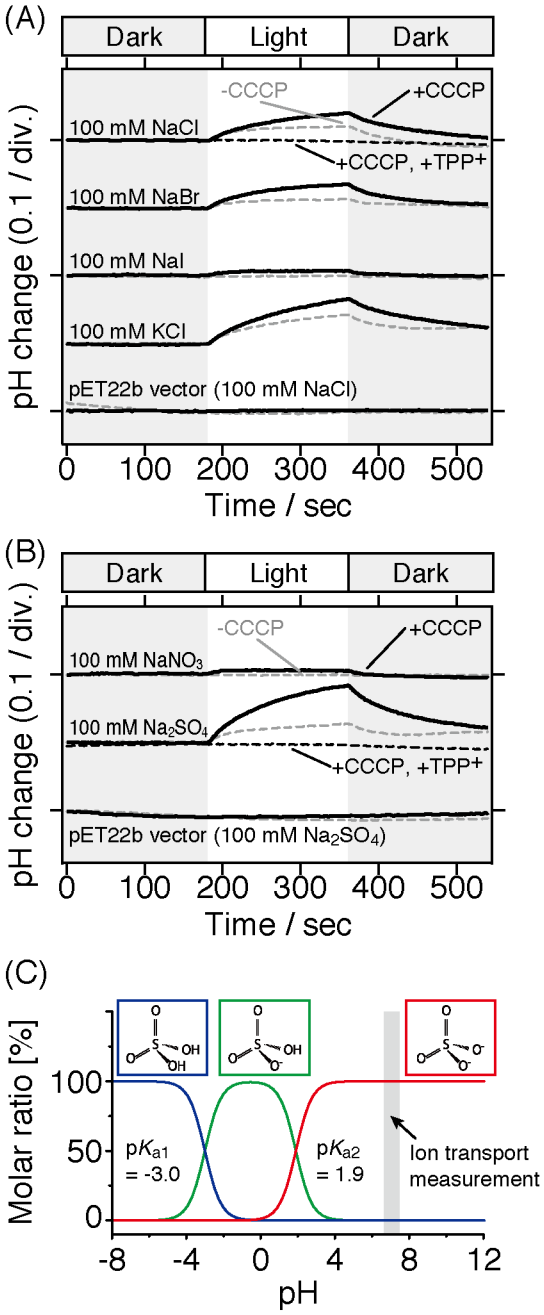
(A)
Dark
Light
Dark
-CCCP
+CCCP
100 mM NaCl
+CCCP, +TPP+
100 mM NaBr
100 mM NaI
100 mM KCl
pET22b vector (100 mM NaCl)
pH change (0.1 / div.)
0
100
200
300
400
500
Time / sec
(B)
Dark
Light
Dark
-CCCP
+CCCP
100 mM NaNO3
100 mM Na2SO4
+CCCP, +TPP+
pET22b vector (100 mM Na2SO4)
pH change (0.1 / div.)
0
100
200
300
400
500
Time / sec
(C)
Molar ratio [%]
100
50
0
pKa1
= -3.0
pKa2
= 1.9
Ion transport
measurement
-8
-4
0
4
8
12
pH

Figure3

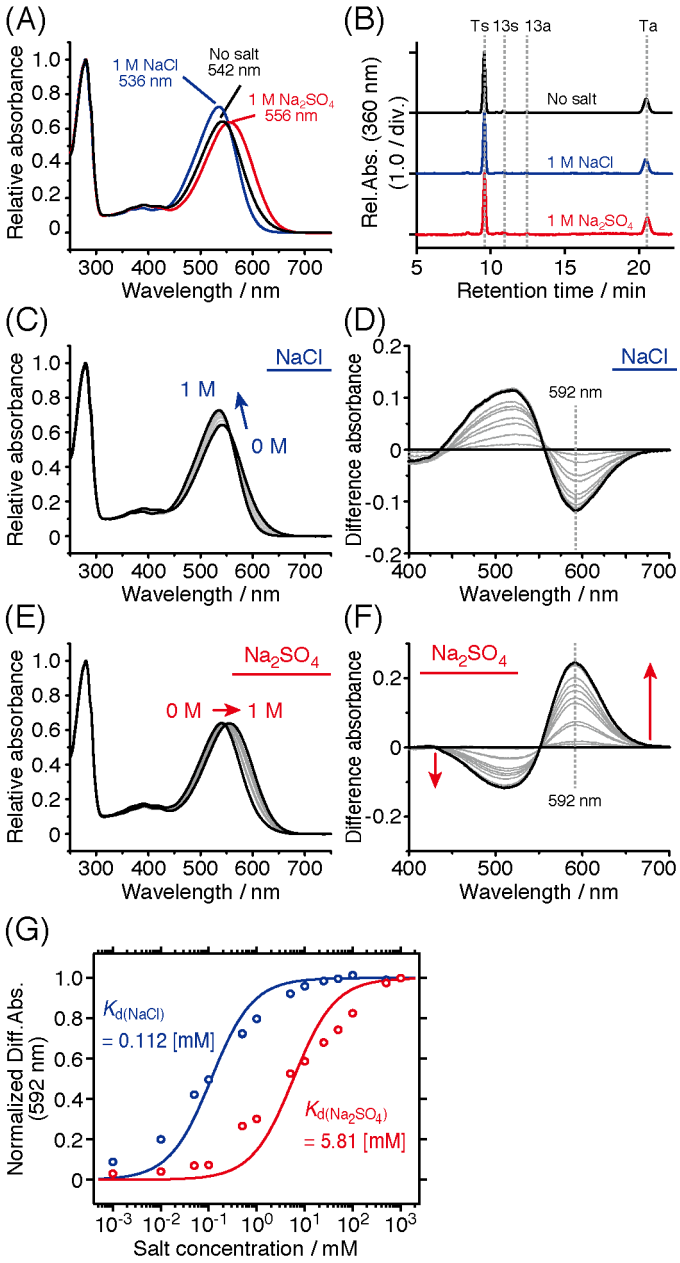
(A)
Relative absorbance
1 M NaCl
536 nm
No salt
542 nm
1 M Na2SO4
556 nm
Wavelength / nm
(B)
Ts 13s 13a
Ta
No salt
1 M NaCl
1 M Na2SO4
Rel.Abs. (360 nm)
(1.0 / div.)
Retention time / min
(C)
NaCl
1 M
0 M
Relative absorbance
Wavelength / nm
(D)
NaCl
592 nm
Difference absorbance
Wavelength / nm
(E)
Na2SO4
0 M → 1 M
Relative absorbance
Wavelength / nm
(F)
Na2SO4
592 nm
Difference absorbance
Wavelength / nm
(G)
Kd(NaCl)
= 0.112 [mM]
Kd(Na2SO4)
= 5.81 [mM]
Normalized Diff.Abs.
(592 nm)
Salt concentration / mM

Figure4

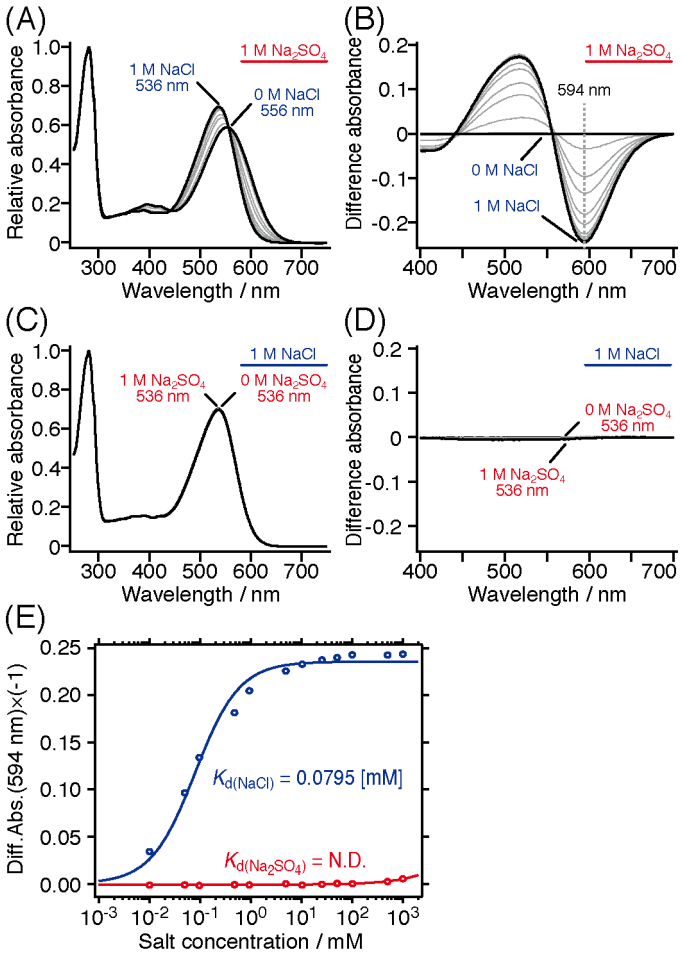
(A)
Relative absorbance
1.0
0.8
0.6
0.4
0.2
0
1 M NaCl
536 nm
1 M Na2SO4
0 M NaCl
556 nm
300 400 500 600 700
Wavelength / nm
(B)
Difference absorbance
0.2
0.1
0
-0.1
-0.2
1 M Na2SO4
594 nm
0 M NaCl
1 M NaCl
400 500 600 700
Wavelength / nm
(C)
Relative absorbance
1.0
0.8
0.6
0.4
0.2
0
1 M NaCl
1 M Na2SO4
536 nm
0 M Na2SO4
536 nm
300 400 500 600 700
Wavelength / nm
(D)
Difference absorbance
0.2
0.1
0
-0.1
-0.2
1 M NaCl
0 M Na2SO4
536 nm
1 M Na2SO4
536 nm
400 500 600 700
Wavelength / nm
(E)
Diff.Abs.(594 nm)×(-1)
0.25
0.20
0.15
0.10
0.05
0.00
Kd(NaCl) = 0.0795 [mM]
Kd(Na2SO4) = N.D.
10-3 10-2 10-1 100 101 102 103
Salt concentration / mM

Figure5

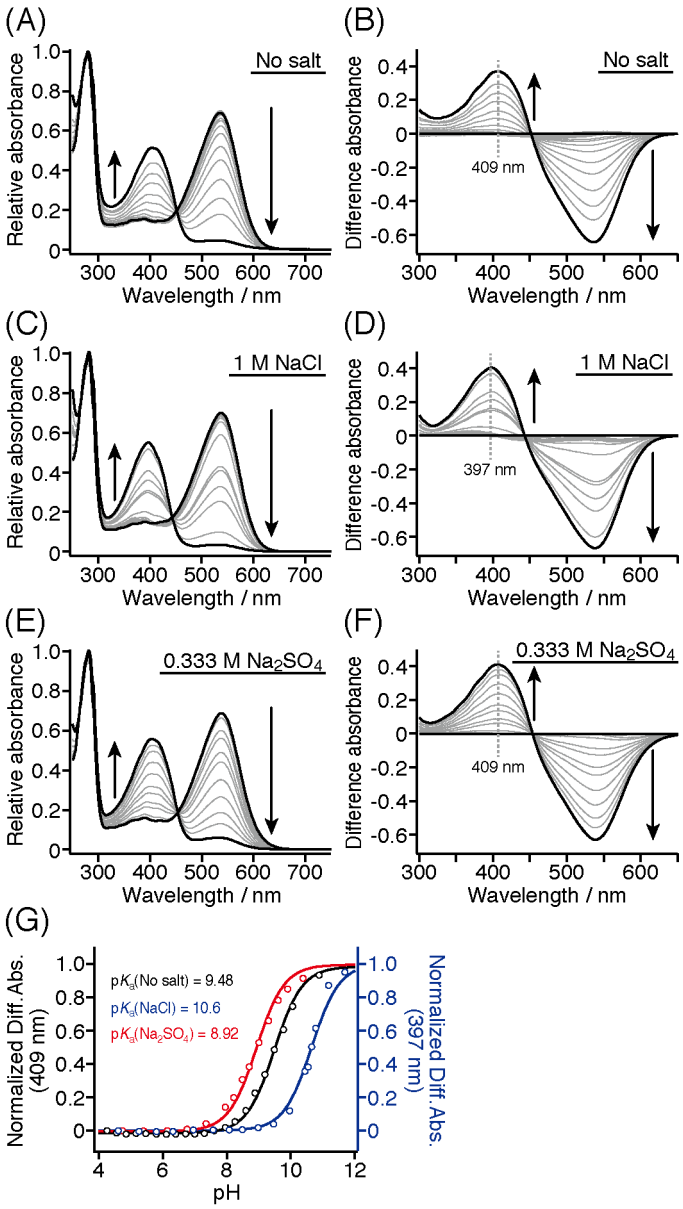
(A)
No salt
Relative absorbance
Wavelength / nm
(B)
No salt
409 nm
Difference absorbance
Wavelength / nm
(C)
1 M NaCl
Relative absorbance
Wavelength / nm
(D)
1 M NaCl
397 nm
Difference absorbance
Wavelength / nm
(E)
0.333 M Na2SO4
Relative absorbance
Wavelength / nm
(F)
0.333 M Na2SO4
409 nm
Difference absorbance
Wavelength / nm
(G)
pKa(No salt) = 9.48
pKa(NaCl) = 10.6
pKa(Na2SO4) = 8.92
Normalized Diff. Abs. (409 nm)
Normalized Diff. Abs. (397 nm)
pH

Figure6

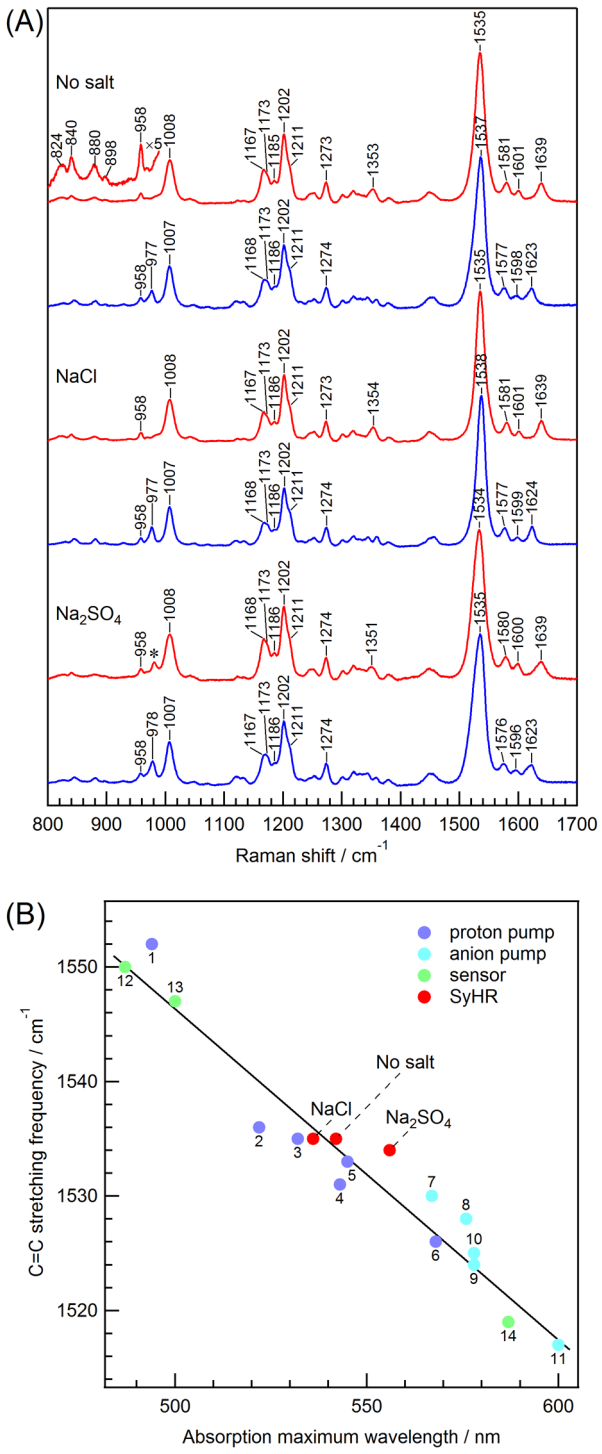
(A)
No salt
824
840
880
898
958
1008
1167
1173
1185
1202
1211
1273
1353
1535
1537
1581
1601
1639
958
977
1007
1168
1186
1173
1202
1211
1274
1535
1577
1598
1623
NaCl
958
1008
1167
1173
1186
1202
1211
1273
1354
1538
1581
1601
1639
958
977
1007
1168
1173
1186
1202
1211
1274
1534
1577
1599
1624
Na2SO4
958
*
1008
1168
1173
1186
1202
1211
1274
1351
1535
1580
1600
1639
958
978
1007
1167
1173
1186
1202
1211
1274
1576
1596
1623
800
900
1000
1100
1200
1300
1400
1500
1600
1700
Raman shift / cm-1
(B)
proton pump
anion pump
sensor
SyHR
No salt
NaCl
Na2SO4
1
2
3
4
5
6
7
8
9
10
11
12
13
14
1550
1540
1530
1520
C=C stretching frequency / cm-1
500
550
600
Absorption maximum wavelength / nm

Figure7

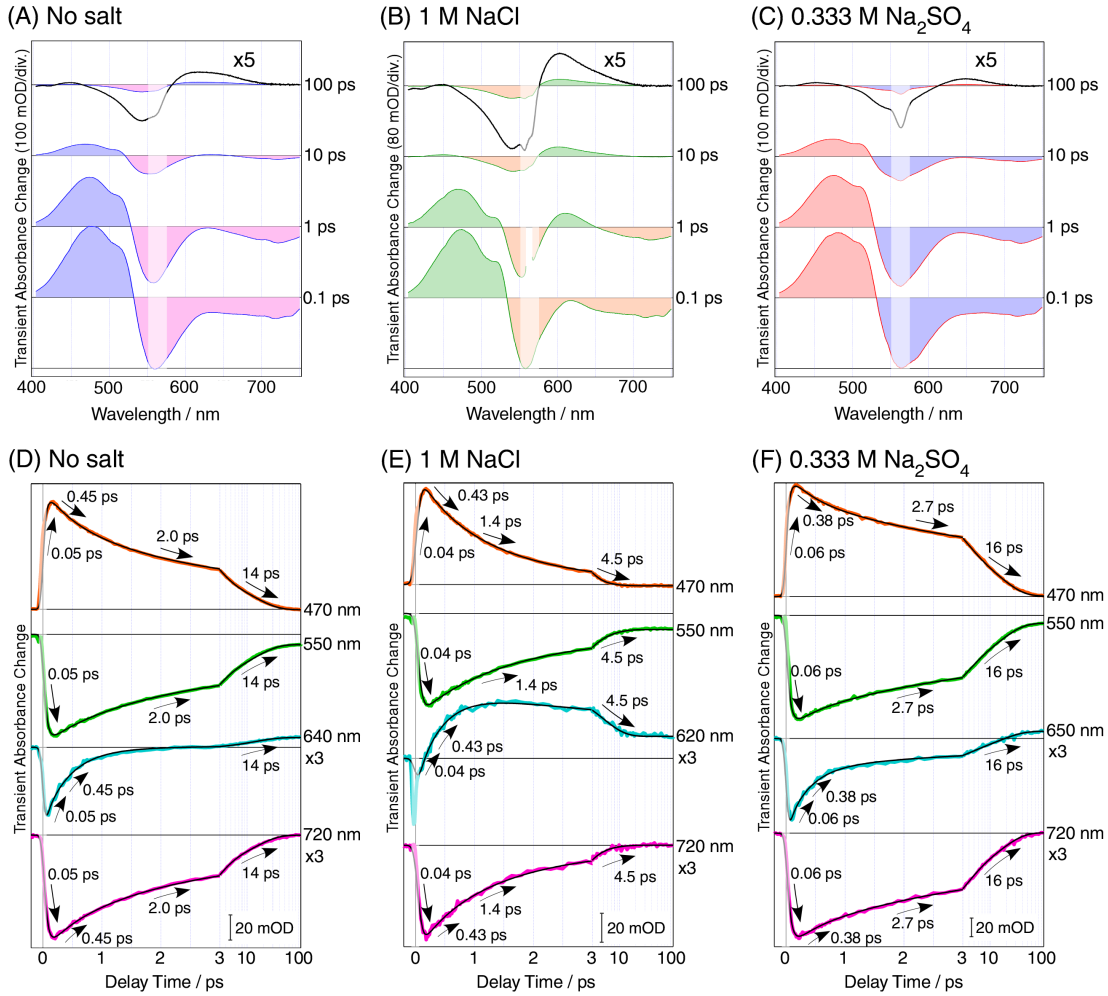
(A) No salt
(B) 1 M NaCl
(C) 0.333 M Na2SO4
Transient Absorbance Change (100 mOD/div.)
Transient Absorbance Change (80 mOD/div.)
x5
100 ps
10 ps
1 ps
0.1 ps
400 500 600 700
Wavelength / nm
(D) No salt
(E) 1 M NaCl
(F) 0.333 M Na2SO4
Transient Absorbance Change
0.45 ps
0.05 ps
2.0 ps
14 ps
470 nm
550 nm
640 nm
720 nm
x3
0.43 ps
1.4 ps
0.04 ps
4.5 ps
620 nm
0.38 ps
0.06 ps
2.7 ps
16 ps
650 nm
20 mOD
0 1 2 3 10 100
Delay Time / ps

Figure8

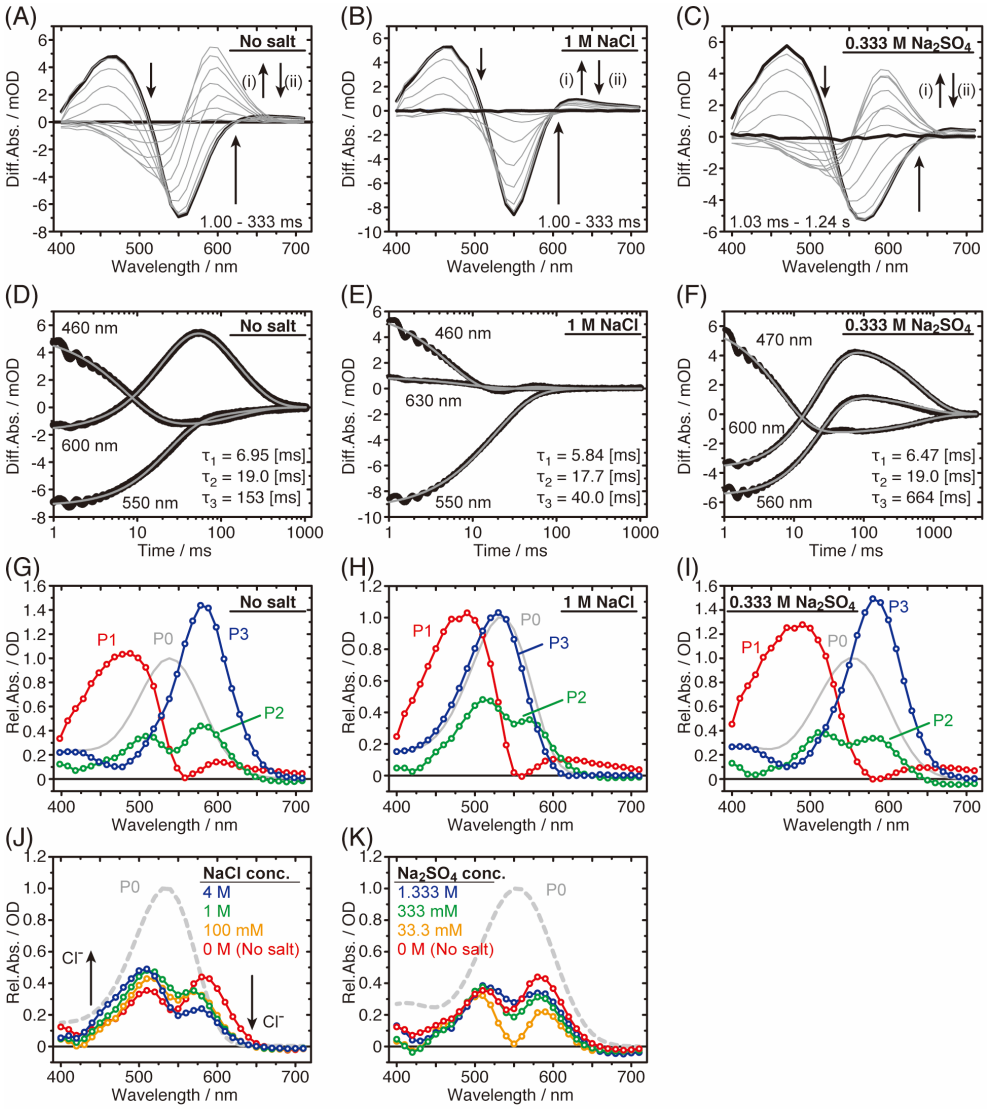
(A)
No salt
(i)
(ii)
1.00 - 333 ms
Diff.Abs. / mOD
Wavelength / nm
(B)
1 M NaCl
(i)
(ii)
1.00 - 333 ms
Diff.Abs. / mOD
Wavelength / nm
(C)
0.333 M Na2SO4
(i)
(ii)
1.03 ms - 1.24 s
Diff.Abs. / mOD
Wavelength / nm
(D)
460 nm
No salt
600 nm
550 nm
τ1 = 6.95 [ms]
τ2 = 19.0 [ms]
τ3 = 153 [ms]
Diff.Abs. / mOD
Time / ms
(E)
460 nm
1 M NaCl
630 nm
550 nm
τ1 = 5.84 [ms]
τ2 = 17.7 [ms]
τ3 = 40.0 [ms]
Diff.Abs. / mOD
Time / ms
(F)
470 nm
0.333 M Na2SO4
600 nm
560 nm
τ1 = 6.47 [ms]
τ2 = 19.0 [ms]
τ3 = 664 [ms]
Diff.Abs. / mOD
Time / ms
(G)
No salt
P1
P0
P3
P2
Rel.Abs. / OD
Wavelength / nm
(H)
1 M NaCl
P1
P0
P3
P2
Rel.Abs. / OD
Wavelength / nm
(I)
0.333 M Na2SO4
P1
P0
P3
P2
Rel.Abs. / OD
Wavelength / nm
(J)
NaCl conc.
4 M
1 M
100 mM
0 M (No salt)
P0
Cl⁻
Cl⁻
Rel.Abs. / OD
Wavelength / nm
(K)
Na2SO4 conc.
1.333 M
333 mM
33.3 mM
0 M (No salt)
P0
Rel.Abs. / OD
Wavelength / nm

Figure9

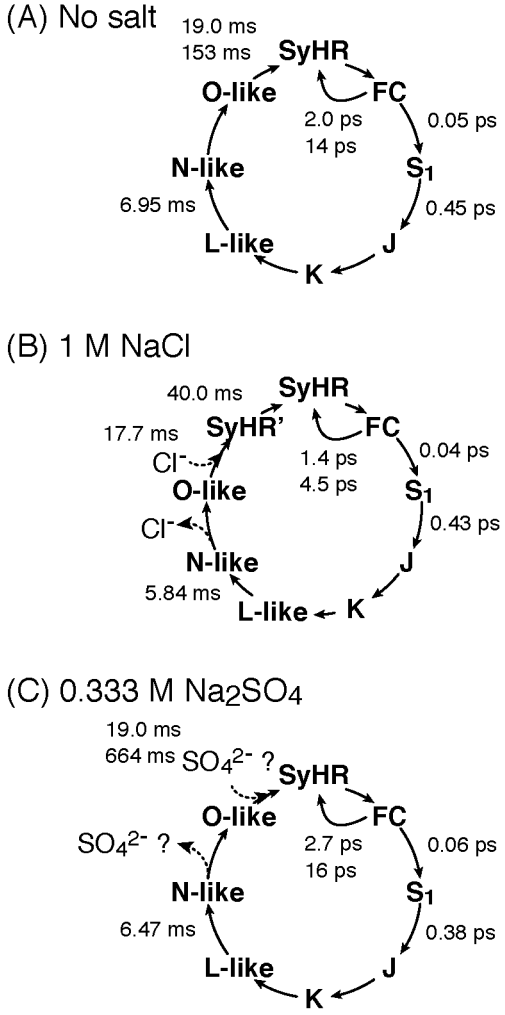
(A) No salt
19.0 ms
153 ms
SyHR
FC
O-like
2.0 ps
14 ps
0.05 ps
S1
N-like
6.95 ms
0.45 ps
L-like
J
K
(B) 1 M NaCl
40.0 ms
SyHR
SyHR'
FC
17.7 ms
Cl-
1.4 ps
4.5 ps
0.04 ps
O-like
S1
Cl-
0.43 ps
N-like
J
5.84 ms
L-like
K
(C) 0.333 M Na2SO4
19.0 ms
664 ms
SO4 2- ?
SyHR
O-like
FC
SO4 2- ?
2.7 ps
16 ps
0.06 ps
N-like
S1
6.47 ms
0.38 ps
L-like
J
K

Figure10

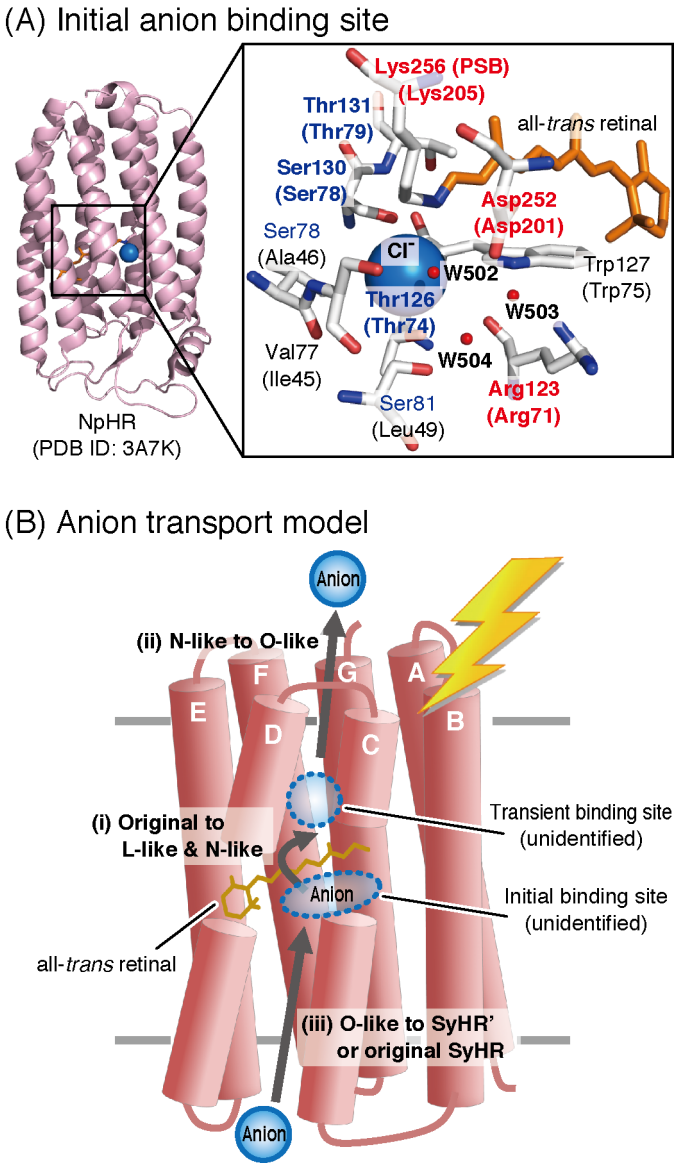
(A) Initial anion binding site
Lys256 (PSB)
(Lys205)
Thr131
(Thr79)
all-trans retinal
Ser130
(Ser78)
Asp252
(Asp201)
Ser78
(Ala46)
Cl-
W502
Trp127
(Trp75)
Thr126
(Thr74)
W503
Val77
(Ile45)
W504
Arg123
(Arg71)
Ser81
(Leu49)
NpHR
(PDB ID: 3A7K)
(B) Anion transport model
Anion
(ii) N-like to O-like
F
G
A
E
D
C
B
Transient binding site
(unidentified)
(i) Original to
L-like & N-like
Anion
Initial binding site
(unidentified)
all-trans retinal
(iii) O-like to SyHR'
or original SyHR
Anion